Fabrication of durable superhydrophobic coatings based on a novel branched fluorinated epoxy

Kai Zhu, Jinwei Zhang, Hao Zhang, Haochen Tan, Wanqiang Zhang, Yibin Liu, Hepeng Zhang, Qiuyu Zhang

PII: S1385-8947(18)31155-0
DOI: https://doi.org/10.1016/j.cej.2018.06.116
Reference: CEJ 19327

To appear in: *Chemical Engineering Journal*

Received Date: 16 March 2018
Revised Date: 15 June 2018
Accepted Date: 18 June 2018

Please cite this article as: K. Zhu, J. Zhang, H. Zhang, H. Tan, W. Zhang, Y. Liu, H. Zhang, Q. Zhang, Fabrication of durable superhydrophobic coatings based on a novel branched fluorinated epoxy, *Chemical Engineering Journal* (2018), doi: https://doi.org/10.1016/j.cej.2018.06.116

Fabrication of durable superhydrophobic coatings based on a novel branched fluorinated epoxy

Kai Zhu[a], Jinwei Zhang[a], Hao Zhang[a], Haochen Tan[a], Wanqiang Zhang[a], Yibin Liu[a], Hepeng Zhang[a,b,*], Qiuyu Zhang[a]

a School of Sciences, Northwestern Polytechnical University, Xi'an 710129, PR China

b Research & Development Institute of Northwestern Polytechnical University in Shenzhen, Shenzhen 518057, PR China

*****Corresponding authors at: School of Applied and Natural Sciences, Northwestern Polytechnical University, Xi'an, 710129, PR China.

E-mail addresses: zhanghepeng@nwpu.edu.cn (H. Zhang)

ABSTRACT:

Low durability is a potential Achilles heel for superhydrophobic coatings, which greatly prevents applications of superhydrophobic materials for various daily living activities. In this paper, a novel branched epoxy, dangling long fluoroalkyl tail, was designed and synthesized. The coating shows contact angles of 165°, 147° and 144° to water, glycol and colza oil, respectively, and shows superhydrophobicity. This coating is also highly durable, withstanding at least 1000 abrasion cycles under 45 kPa. After abrasion testing, its contact angle to water is maintained at 152°. Furthermore, this coating also shows a remarkable stability towards strong acid, UV light, thermal and smudge treatment without apparently losing its superhydrophobicity. The epoxy groups of the T-FAE can form high crosslinking network by the ring-opening reaction and reacting with the Si-OH and -NH_2, and long-fluorine chain offers low surface

energy. All these are responsible for the excellent performance of the coating.

Keywords: Branched epoxy; Superhydrophobic; Thiol-ene click chemistry; Stability

1. Introduction

Superhydrophobic surfaces widely exist in natural organisms, such as lotus leaves[1], rice leaves[1], water strider legs[2, 3], and butterfly wings[4]. Those surfaces showing a water contact angle (WCA) over 150° and a sliding angle (WSA) lower than 10°[5-7] have attracted attention from many scientists since the last century. Benefitting from the special surface properties, such surfaces gave tremendous applications in anti-fouling[8], self-cleaning[9-11], anti-icing[12-14], anti-corrosion[15-17], anti-drag[18, 19], water-oil separation[20-23] and other fields. Inspired by natural lotus leaves, researchers have recognized that the coexistence of wax and microscale papillae is key for realizing a superhydrophobic surface. In other words, materials with low surface energy and a micro-/nanostructure can be used to create a superhydrophobic surfaces[24].

With the development of superwetting materials, a large number of methods have been proposed to fabricate artificial superhydrophobic surfaces, most of which, however, require tedious procedures, such as the phase separation method[25], template method[26, 27], electrochemical method[28], electrospinning[29, 30] and ion-assisted deposition methods[31]. Recently, thiol-ene chemistry has been demonstrated to be a better method for the fabrication of superhydrophobic surfaces [32-34]. Bradley et al. have reported a simple spray coating technique followed by

subsequent photopolymerization for the preparation of superhydrophobic coatings based on nanoparticle-laden thiol-ene resins[35].

Although these miraculous surfaces have been thoroughly studied over the last hundred years, low mechanical and adhesion strength still hinder their wide utilization in our daily lives [36-41]. Most superhydrophobic coatings have low resistance to harsh physical insults ranging from a knife scratch, sandpaper abrasion, washing and even pouring rain water. Xue et al. successfully prepared robust superhydrophobic surfaces using (heptadecafluoro-1,1,2,2-tetrahydrodecyl) trimethoxysilane tetraethyl orthosilicate and a trimer of hexamethylene diisocyanate. Although this coating can bear 200 abrasion cycles under 2 kPa with 2000 mesh sandpaper and remain superhydrophobic, it still cannot meet the needs practical applications[42]. Chen et al. discovered that a spray adhesive could be used to promote the robustness and adhesion strength of the coating; however, this method is not suitable for all kinds of substrates[43]. Until now, although many kinds of methods have been proposed to enhance adhesion forces between substrate and coating, almost no research exists for improving adhesion through the design and preparation of functional monomers.

In this paper, a novel branched epoxy named T-FAE was designed and synthesized; an epoxy group and long-fluorine hydrophobic group were introduced into the same molecule by base-catalyzed thiol-ene Michael addition reaction of pentaerythritol tetra(3-mercaptopropionate) (PETMP), glycidyl methacrylate (GMA) and [N-methyl-perfluorohexane-1-sulfonamide] ethyl acrylate (PFSA). The self-designed T-FAE contains both a long-fluorine chain and epoxy groups, offering

low surface energy and chemical reactivity, respectively. Moreover, the epoxy groups can also form a robust crosslinking network after curing and improve the adhesive strength between the substrate and coating, which increases the mechanical performance of the coatings. Benefitting from T-FAE, a superhydrophobic coating with excellent stability was fabricated after mixing 1-benzyl-2-methyl-1H-imidazole (BMI), curing agent, and silicon dioxide with T-FAE. In addition, γ-aminopropyltriethoxysilane (APTES) was also introduced into the system to further enhance the robustness and adhesion force, as the amidogen and silicon hydroxyl groups, which are transformed from the alkoxy groups, can react with T-FAE. This coating is highly robust and capable of withstanding at least 1000 abrasion cycles under 45 kPa. After abrasion testing, the contact angle to water is still maintained at 152°, with the coating also demonstrating remarkable durability towards strong acid, UV light, thermal and smudge treatment without losing its superhydrophobicity.

2. Experimental section

2.1 Materials

[N-Methyl-perfluorohexane-1-sulfonamide] ethyl acrylate (PFSA), Dimethylphenyl phosphine (DMPPh) and γ-aminopropyltriethoxysilane (APTES) was purchased from Sigma-Aldrich. 2-hydroxy-2-methylpropiophenone (HMPP), Glycidyl methacrylate (GMA) and 1-benzyl-2-methyl-1H-imidazole (BMI) were all obtained from TCL. Pentaerythritol tetra (3-mercaptopropionate) (PETMP) was bought from Evans Chemetics. Other reagents, such as acetone and sodium hydroxide,

were obtained from J & K at the highest purity available and were used without further purification unless otherwise specified. Commercial fabrics (100% polyester) were purchased from a local supermarket.

2.2 Preparation of T-FAE

In this paper, novel branched T-FAE monomers were synthesized using two different methods: a base-catalyzed method and a thiol-radical click chemistry method. The preparation processes are described as follows:

2.2.1 Base-catalyzed method

A novel branched T-FAE was realized via a base-catalyzed thiol-ene Michael addition reaction (Fig. 1). 4.26 g GMA was mixed with 4.88 g PETMP and 5.11 g PFSA, with a molar ratio of 3:1:1; then, acetone, with the same mass as the total amount of reactants (14.25 g), was added. Next, the mixture was treated using ultrasonication for 10 min, and 0.0713 g DMPPh was added into the obtained homogenous solution under a normal air atmosphere, followed by a further reaction for 6 hours at 25 °C.

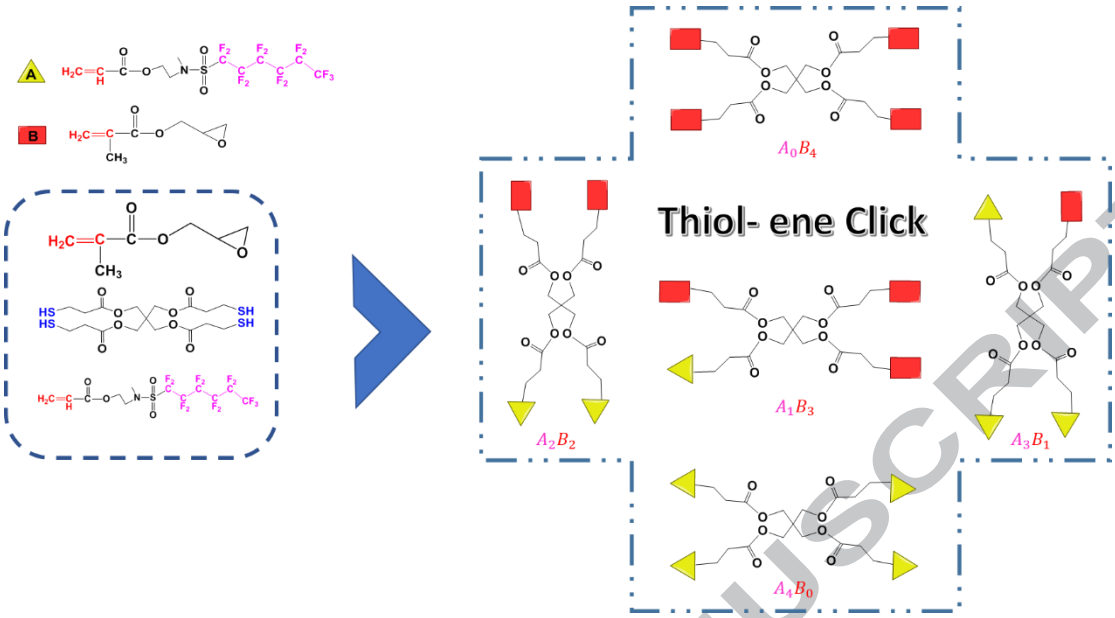

Fig. 1. The scheme used for preparing T-FAE via the thiol-ene click method

2.2.2 Thiol-radical click chemistries method

A novel branched T-FAE was realized via a thiol-radical click chemistries reaction. 4.26 g GMA was mixed with 4.88 g PETMP and 5.11 g PFSA, with a molar ratio of 3:1:1; then, acetone, with the same mass as the total amount of reactants (14.25 g), was added. Next, the mixture was treated using ultrasonication for 10 min before adding 0.1425 g HMPP into the obtained homogenous solution under ultraviolet radiation, followed by a further reaction for 1 hour at 25 °C.

2.3 Preparation of the superhydrophobic coating

First, 1 g branched T-FAE (50 wt% in acetone solution), 12.5 mg BMI, APTES and SiO_2 were mixed together in acetone (the same mass as the total amount of the reactants) and then ultrasonicated for 20 min to form homogenous solution. The weight ratios for APTES/T-FAE were varied from 0 to 1/5 (0, 1/20, 1/15, 1/10, 1/5), while the addition of SiO_2 ranged from 0 to 0.2 g (0.05 g as a unit). A PET fabric

(P-fabric) was coated using the as-prepared coating solution for 5 min using a dip-coating method and then cured at 120 °C and 150 °C, each for one hour.

2.4 Characterization

2.4.1 Mechanical Durability Tests

These tests were carried out according to the modified AATCCA Test Method 8-2001. In these tests, the coated-fabric (C-fabric, also called fabric@F-B(A)-S) was fixed onto a stainless-steel column and moved repeatedly under a pressure of 45 kPa at a speed of 60 cycles/min (20 cm for a cycle). The P-fabric was used as the test interface.

Fig. S1 shows the scheme of the sandpaper abrasion test. The prepared sample weighing 200 g was placed face-down to 800 grid SiC sandpaper. We moved for 10 cm along the ruler, then rotated the sample for 90° and moved for another 10 cm along the ruler in the opposite direction. This process was defined as one cycles.

The jet impact test was carried out as the following method: a nozzle with inner diameter of 6 mm was connected to the faucet. Then the prepared sample fixed by a fixture was placed in the sink, and the distance between the surface of the sample and the nozzle was 35 cm. With the faucet moving to maximal, the sample was carved by the high-speed flow (the initial velocity of the flow was about 1.2m/s) for 3 h.

2.4.2 Chemical stability tests

Water droplets (8 μl) with different pH values ranging from 1 to 14 were placed onto the surface of the C-fabric to test the chemical stability of the superhydrophobic coatings.

Chemical stability of the C-fabric was further tested by immersing the samples in strong acid (H_2SO_4, pH = 1) or base solutions (KOH, pH = 14) at room temperature for 1 to 4 hours (1 hour as a unit). Every hour, pars of the samples were taken out, rinsed with distilled water for 3 min, dried in an oven at 70 °C for 10 min followed by a recording of the water contact angles (WCA) for the samples.

2.4.3 UV tests.

For the *UV*-durability test, the C-fabric surface was continuously illuminated by a UV lamp (wavelength of 365 nm) from a distance of 15 cm for 4 hours.

2.4.4 Stain resistance tests

The contamination solution for the samples was prepared as follows: a packet of instant coffee (15 g) was dissolved in 150 mL boiling water and then cooled to room temperature. Subsequently, a piece of the sample was immersed into the contamination solution, and photographs of the testing sample were taken every 1 hour.

2.4.5 Other characterization

IR data were obtained using a TENSOR-27 Fourier transform infrared spectrometer (Bruker) operating over the frequency range of 4000–450 cm^{-1}. ^{1}H-NMR spectra were observed using a Bruker Avance III-400 NMR spectrometer with a 4-mm fused zirconia solid probe. Deuterated chloroform was used as solvent and TMS used as an internal standard. The morphology of the coatings was characterized by a scanning electron microscope (SEM, JEOL JSM – 6700F) equipped with an energy-dispersive spectroscope (EDS, Oxford). The surface chemical composition and elemental

distribution for the coatings was investigated using a Kratos AXIS Ultra DLD spectrometer at a 90 °C take off angle equipped with a 300 W monochromatic Al Kα X-ray source. Thermal gravimetric (TG) analyses of the neat-epoxy resin was carried out at 10 °C/min (oxygen atmosphere), over the whole range of temperature (25-800 °C) by SDTQ600 (Waters-TA, American). Water, glycol and colza oil contact angles (CA) for 8 μL droplets and sliding angles (SA) for 45 μL droplets were measured using a PT-705C contact angle meter. All the CA and SA values were averages of 3 tests and were recorded at different sample positions.

3. Results and discussion

3.1 Preparation and Characterization of T-FAE

T-FAE was manufactured by the base-catalyzed method and thiol-radical click chemistry method, with the mechanisms for the two methods illustrated in Fig. 2a. The radical reaction is very rapid; however, the characteristic absorption band for the thiol groups at 2570 cm^{-1} still exists in the infrared spectrum of the radical reaction product, while no such peak is observed in the Michael-product (Fig. 2b). In addition, the peak at 1640 cm^{-1} corresponding to the C=C bonds disappears in both the radical-product and Michael-product. This result indicates that the -SH groups were not completely consumed but that the C=C bonds all reacted in the radical system, which may be caused by radical polymerization of the vinyl monomers thus, the base-catalyzed method was chosen in the following experiments to prepare the branched T-FAE, which exhibits a rapid, quantitative conversion with no byproducts.

The chemical structure for T-FAE was confirmed by FT-IR and ^{1}H-NMR. The

typical IR spectra for the reactants (mixture of PETMP, GMA and PFSA) and products (T-FAE) are compared in Fig. 2b. A relatively weak absorption peak at 907 cm^{-1} resulting from the epoxy group is observed in all the samples. In addition, the band at 1740 cm^{-1} is attributed to C=O stretching vibrations of the ester groups, and the peaks at 1210 cm^{-1} and 1100 cm^{-1} correspond to the $-CF_2-$ and $-SO_2-$ groups, respectively. Compared to the IR spectrum of the reactants, the peaks centered at 2569 cm^{-1} and 1640 cm^{-1} attributed to -SH and C=C stretching vibrations all disappear and the peaks between 2850 cm^{-1} and 3000 cm^{-1} ascribed to C-H stretching vibrations increase in the T-FAE obtained by the base-catalyzed method.

Fig. 2c demonstrates the typical ^{1}H-NMR spectra obtained for the reactants and T-FAE. Signals for the vinyl end-group in GMA and PFSA are observed at 5.7-6.4 ppm in the ^{1}H-NMR spectrum of the reactants. After the thiol-ene reaction, the signals at 5.7-6.4 ppm disappear, and the intensities of the peaks at 2.6-2.8 ppm (methylene protons) are enhanced. In addition, the signals for the methyl proton adjacent to the terminal double bond of GMA observed at 1.9 ppm shift quantitatively to 1.2 ppm, which is caused by the change in the chemical state for this methyl proton. All the above data demonstrate that PETMP is modified by GMA and PFSA through the Michael addition reaction and that the designed T-FAE was successfully synthesized, and the yield of T-FAE, measured by ^{1}H-NMR, was more than 99%.

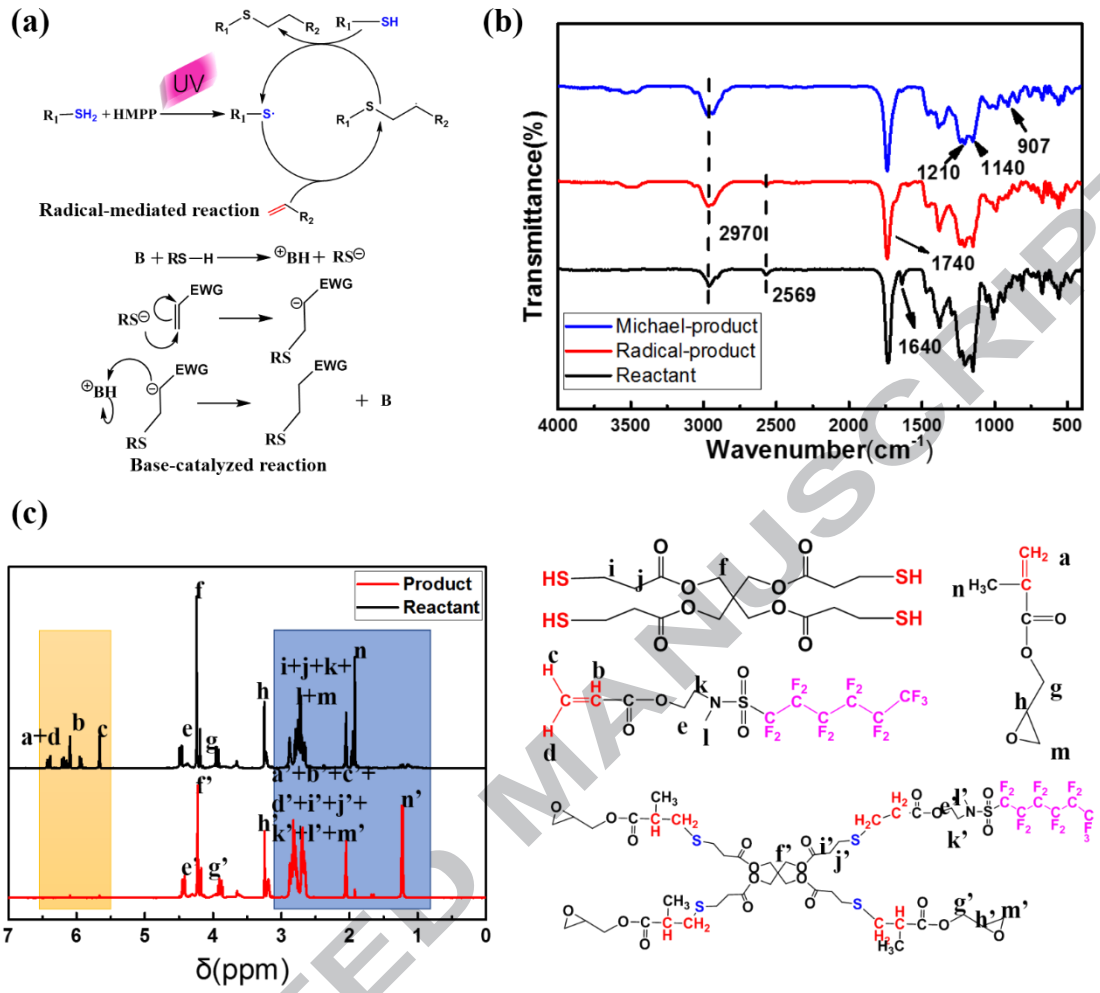

Fig. 2. (a) Preparation mechanisms for T-FAE; (b) FT-IR spectra of the reactants (mixture of PFSA, GMA and PETMP) and T-FAE; (c) Structure and the ^{1}H-NMR spectra of the reactants (mixture of PFSA, GMA and PETMP) and T-FAE

Furthermore, TE, which contained four epoxy groups in one molecule synthesized by base-catalyzed thiol-ene Michael addition reaction of PETMP and GMA, and T-FAE mixed with BMI, coated on the glass surface, and the CA to water were 77° and 104° (Fig. S2), respectively. It could be concluded that long-fluorine hydrophobic group introduced to T-FAE could greatly reduce the interface energy of glass surface and the T-FAE coating made the glass surface hydrophobic.

Thermal property of the novel branched epoxy T-FAE was measured and the

TGA curves of the T-FAE cured by the BMI was showed in Fig. S3. Thermal degradation onset temperature for sample was about 165 °C，and the major weight loss of sample was between 300 °C and 450 °C.

3.2 Wetting behavior and mechanical durability

Fig. 3 illustrates the preparation process for the coating. T-FAE and BMI, the major ingredients in the coating, were solved in acetone (Fig. 3 via1) to form the curing system. Moreover, APTES and hydrophobic-SiO_2 particles (average size of silica particles was 16 nm) were added into the above system (Fig. 3 via2) to improve the adhesion force and roughness of the surface. The T-FAE as a main ingredient in these coatings contains many epoxy groups, which can form high crosslinking network by reacting with the Si-OH and -NH_2 and the ring-opening reaction, and this is responsible for the great mechanical durability of the coating. Besides, the sol-gel reaction to form Si-O-C bonds between APTES and substrate also presents high adhesion that is also promoted by the C-O-C bonds between the T-FAE and P-fabric. These lead to robust super-repellency coating. In addition, hydrophobic-SiO_2 particles are able to improve the roughness of the surface, which is vital for realizing superhydrophobicity. To simplify the subsequent state, the T-FAE and BMI system is called F-B, the T-FAE, BMI and APTES system is named F-B(A) and the T-FAE, BMI, APTES and SiO_2 system will be marked as F-B(A)-S.

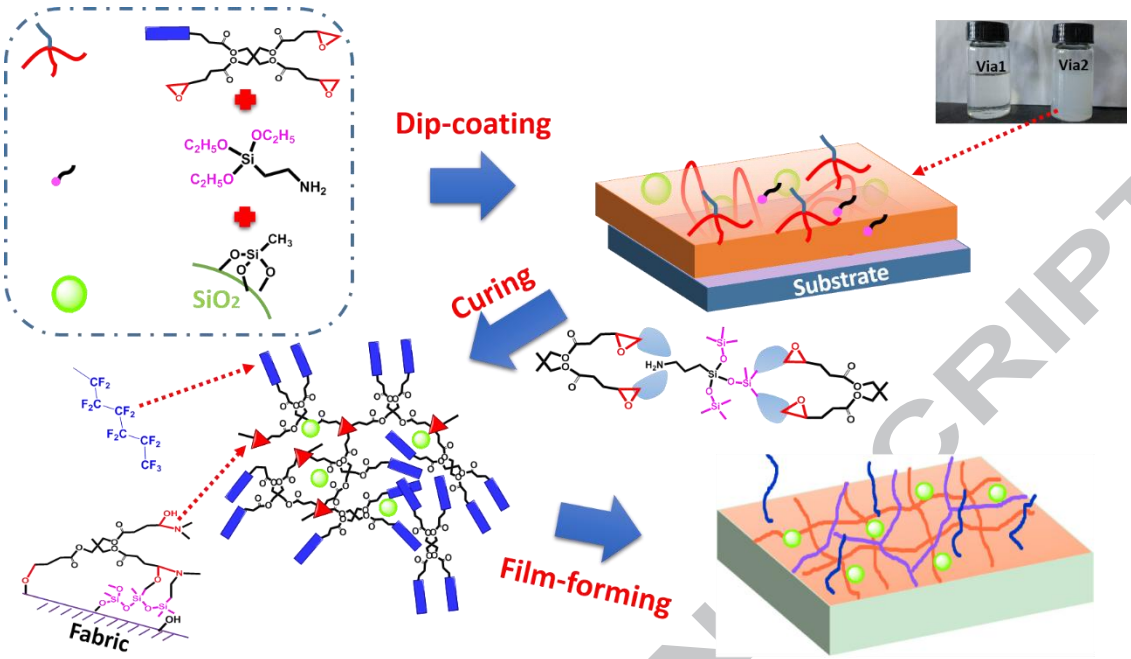

Fig. 3. The preparation mechanism and procedure used for the coating and the structure of the cured resin.

The super-repellency of the coatings was assessed by measuring the CA for both low and high surface tension liquids, including water, glycol and colza oil. The results are shown in Fig. 4. The CA to water and glycol for the F-B coating is 148° and 144°, respectively. The CA (Fig. 4a-b) and SA (Fig. S4) shows no obvious changes with increasing APTES amount. However, all the CAs to the three liquids distinctly increase when hydrophobic-SiO_2 particles are added to F-B(A). As the SiO_2 weight ratio increases, the CA increases (Fig. 4c-d, Fig. S5) and the WSA decreases (Fig. S6). The CA of F-B(A)-S to water, glycol and colza oil can increase to 169°, 148° and 144°, respectively, while the WSA decreases to 5° when the addition of SiO_2 particles accounts for 40 wt% of the major ingredient.

The mechanical durability for the three coatings was investigated, with the results shown in Fig. 4. From Fig. 4a, it can be observed that the F-B coating exhibits excellent mechanical properties and that the water contact angle is still maintained at 139° after the mechanical test. Furthermore, the mechanical durability improves when APTES is introduced to the F-B system. For the F-B(A) coatings, the best mechanical durability appears when the weight ratio for APTES: T-FAE is 1:15, with the WCA only decreasing 5° from 148° to 143° after 1000 abrasion tests. The decrease in WCA before and after abrasion is more obvious when SiO_2 is added to F-B(A). Moreover, the mechanical performance of F-B(A)-S is better than that of the F-B and F-B(A) coatings. The CA to water can be maintained at 152° after 1000 abrasion tests when the added amount of SiO_2 is 30 wt% of T-FAE (Fig. 4b). In general, The F-B(A)-S coatings present optimal performance when the ratio APTES: T-FAE is 1:15 and the added amount of SiO_2 is 30 wt% of T-FAE.

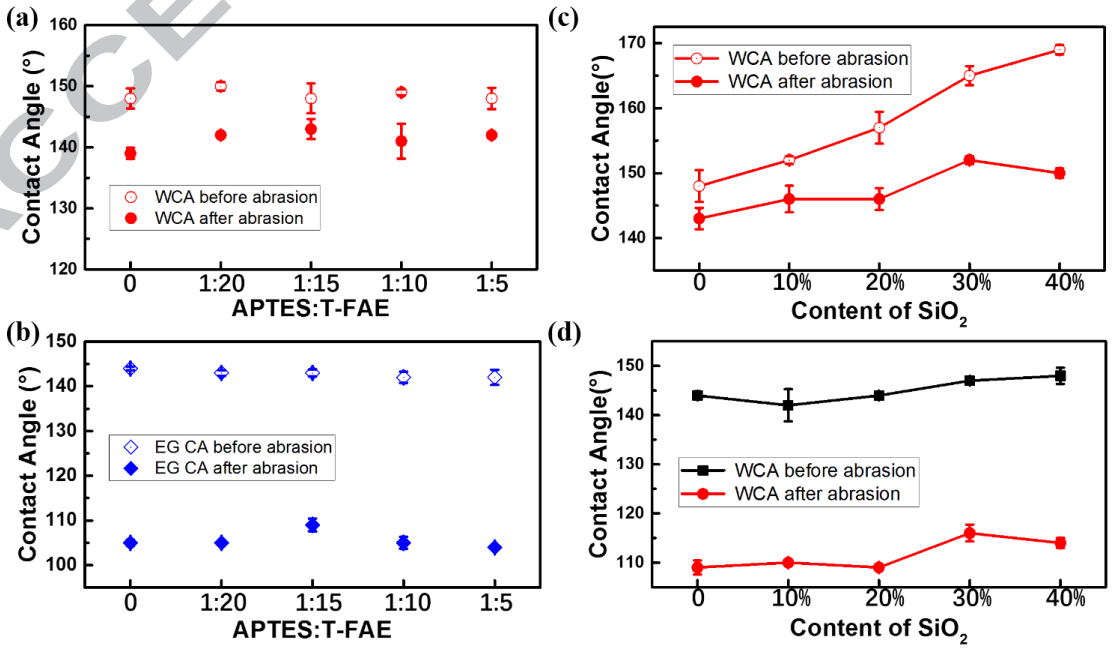

Fig. 4. Influence of the ratio APTES/T-FAE on (a) WCA (b) EG CA before and after 1000 abrasion cycles; influence of SiO_2 concentration on (c) WCA and (d) EG CA before and after 1000 abrasion cycles.

The wetting behavior and mechanical durability of the optimized coatings was investigated, with the results shown in Fig. 5. As shown in Fig. 5a, the C-fabric is efficient in repelling colored liquid droplets (20 μl) leading to the formation of round-liquid balls on the interface. In particular, the coating shows superhydrophobicity and oleophobicity. The CA to water, glycol and colza oil for the C-fabric is 165° (Fig. 5b), 147° and 144°, respectively. In contrast, when these three kinds of colored liquids were dropped onto the P-fabric, which is amphiphilic (Fig. 5c) in air, the droplets were rapidly soaked into the P-fabric, leaving no observable contact angle (Fig. 5d) except for three colored wet spots as the indicating marks. Furthermore, the super-repellency behavior of the coating is also demonstrated by a water jet-spraying experiment (Movie S1), which shows the immediate bouncing off of the water-spout from the composite solid-liquid-air interface as soon as the water-spout touches the surface; this appears to be the Cassie-Baxter state. Additionally, the dynamic anti-wetting behavior for the fabric@F-B(A)-S is also demonstrated in Fig. S8. The results for the mechanical durability imply that the coating shows outstanding abrasion performance, the data also demonstrates superhydrophobicity even after 1000 abrasion cycles (Fig. 5e). Furthermore, the tests of sandpaper abrasion and water-wash were also carried out to detect the mechanical

durability of superhydrophobic coating and the results were shown in Fig. 5f and 5g, the WCA for the sample have little change after 100 sandpaper abrasion cycles or 3 h water-wash, indicating that this coating is stable to sandpaper abrasion and water-wash.

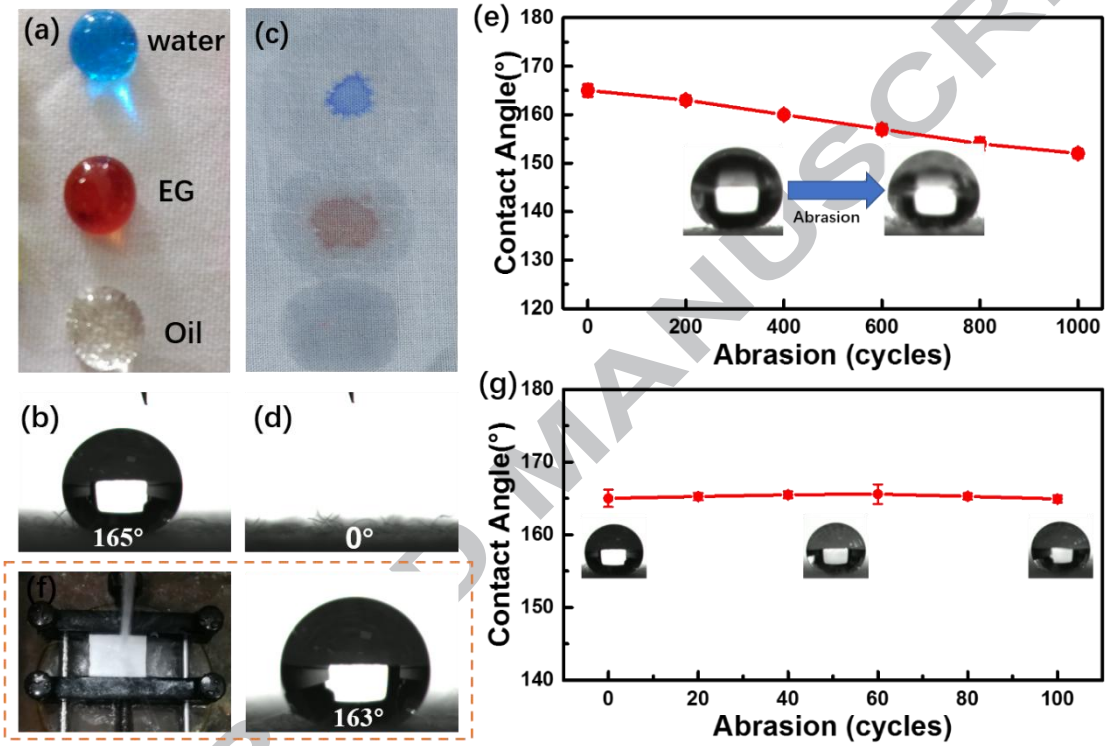

Fig. 5. (a) Digital images of the blue water, red EG and oil on the surface of the C-fabric; (b) WCA of the C-fabric; (c) Digital images of the blue water, red EG and oil on the surface of the P-fabric; (d) WCA of the P-fabric; (e) WCA changes of the fabric@F-B(A)-S with abrasion cycles; (f) Digital images of the C-fabric under water-washing and WCA of the C-fabric after water-washing; (g) WCA changes of the fabric@F-B(A)-S with sandpaper abrasion cycles.

3.3 Surface chemical composition and morphology

The changes in the wetting behavior for the fabrics can be attributed to the variations in their surface morphology and chemical composition. The information for

the morphologies of the P-fabric and C-fabric was analyzed using SEM, with the results shown in Fig. 6. The image for the P-fabric shows that the fibers (diameter: approximately 12 μm) were of cylindrical shape with a smooth surface (Fig. 6a). However, bumps are clearly observed on the surface of the fibers in the fabric@F-B(A)-S (Fig. 6c). These nanoscale bumps in conjunct with the micron sized fibers provide a multi-scale structure, which meets the need for superhydrophobicity, leading to super-repellent behavior for the F-B(A)-S coating. The chemical composition for the fabric@F-B(A)-S were also explored by FTIR and XPS. Fig. S9 shows the ATR-IR spectra for the P-fabric and fabric@F-B(A)-S. A peak at 1012 cm^{-1}, attributed to C-O stretching vibrations, is visible in all samples. The peaks at 1055 cm^{-1} and 810 cm^{-1} only appear for the fabric@F-B(A)-S samples. The former corresponds to C-F stretching vibrations and the latter is ascribed to Si-O-Si stretching vibrations. The differences between the P-fabric and C-fabric imply that an F-B(A)-S coating is successfully introduced onto the surface of the fabric.

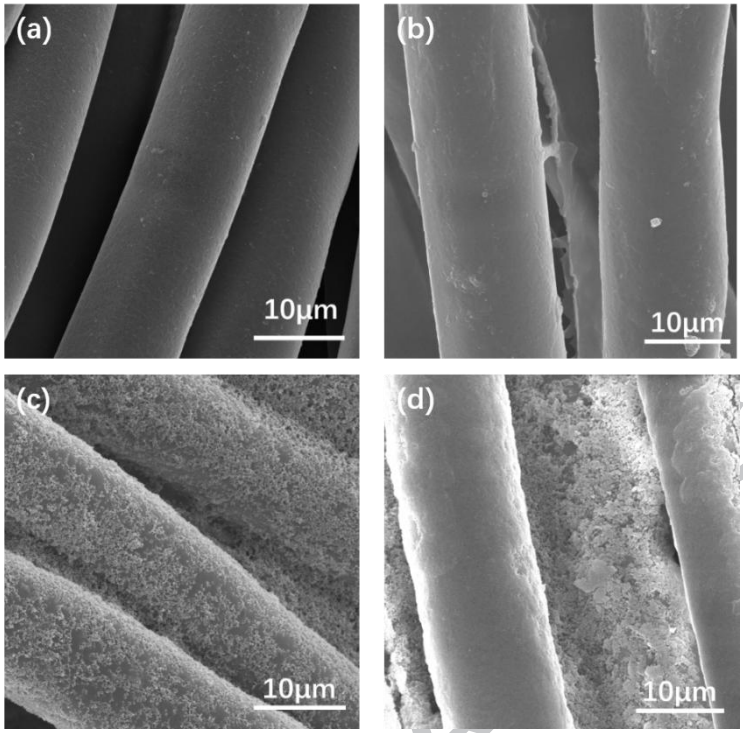

Fig. 6. SEM images for the fabrics: (a) P-Fabric; (b) Fabric@F-B(A); (c) Fabric@F-B(A)-S before abrasion and (d) Fabric@F-B(A)-S after abrasion tests

XPS was also used to verify the chemical compositions in more detail, with Fig. 7a showing the XPS spectra for the P-fabric and C-fabric. It is clear that the P-fabric only consists of C and O elements. After coating, three new peaks appear in the XPS spectra for the C-fabric. The high and sharp peak at approximately 687 eV is attributed to the F element and the two peaks at 101 and 160 eV can be ascribed to Si 2s and Si 2p, respectively. The percentage of C, O, Si and F calculated from the XPS data was 51.1%, 21.4%, 2.3% and 25.2%, respectively. The C 1s spectra were deconvoluted into five component peaks according to the different binding energies between each element, with the results shown in Fig. 7c. The broadest and highest peak at 284.8 eV is ascribed to CH_x (including C-C and C-H), with the other four

peaks respectively corresponding to C-O/C-N/C-S (286.0 eV), C=O (288.2 eV), CF_2 (291.0 eV) and CF_3 (293.3 eV). All these data further verify that F-B(A)-S was successfully coated onto the surface of the fabric. The high WCA for fabric@F-B(A)-S (up to 165°) results from its long-fluorine group and the roughness of the surface, leading to superhydrophobicity for this material.

The morphology of fabric@F-B(A)-S after the abrasion test was also characterized by SEM, with the results shown in Fig. 6d. Most of the SiO_2 particles on the surface of the fibers had peeled off; however, the nanoroughness for the fiber inside remained. The XPS spectra for fabric@F-B(A)-S after the abrasion test (Fig. 7b and d) indicate the existence of four elements (C, O, F and Si), implying that the coating was not seriously destroyed by abrasion. The residual nanoroughness of the abraded fabric@F-B(A)-S results in its high WCA of 152°, with the coating remaining superhydrophobic even after severe abrasion tests.

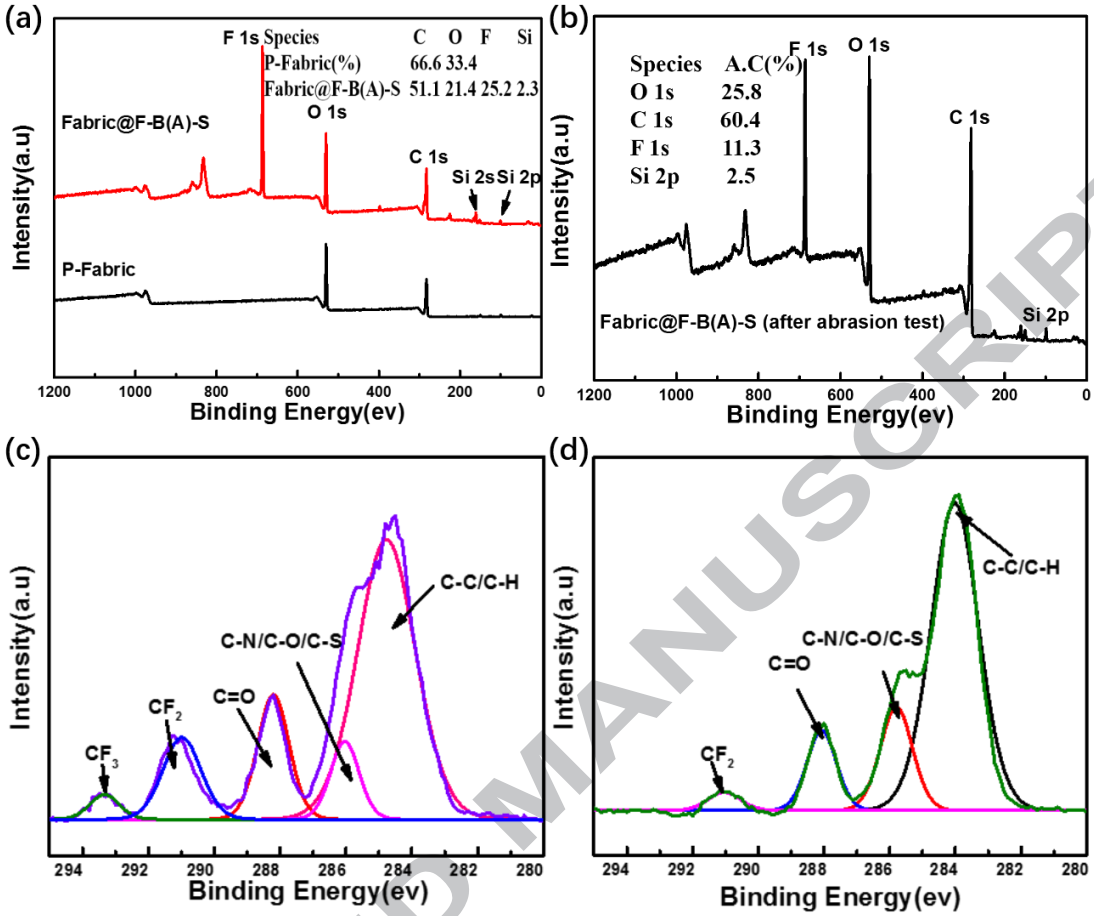

Fig. 7. (a) XPS spectra measured for the P-Fabric and Fabric@F-B(A)-S; (b) XPS spectra for Fabric@F-B(A)-S after abrasion tests; (c) High-resolution C 1s spectra for the Fabric@F-B(A)-S before abrasion tests and (d) High-resolution C 1s spectra for the Fabric@F-B(A)-S after abrasion tests

3.4 Chemical Stability Test

In addition to abrasion stability, anti-corrosion is also very important. Fig. 8a shows the state of different pH droplets residing on the C-Fabric. All the droplets appear to have a ball shape, suggesting that this coating has a super-repellency ability not only for distilled water but also for a corrosive solution.

Further tests for anti-corrosion were also carried out. Fig. 8b shows the state of

C-fabric immersed in H_2SO_4 (pH = 1) for which no soaking phenomenon could be observed over time. The morphology of the immersed fabric@F-B(A)-S is shown in Fig. 8c; the data show that the nanoroughness was not destroyed, which implies that the coating has a superior repellency against H_2SO_4 attack. The stability against acid damage was also certified by the WCA measured following immersion of a film in corrosive solution for 4 hours, as shown in Fig. S10. The excellent acid durability of fabric@F-B(A)-S is ascribed to the fluorinated chains of T-FAE which prevent from the penetration of acid droplets and the outstanding acid resistance of the synthetic resin and SiO_2 nanoparticles.

A test for stability to base solution was also carried out. The states of the C-Fabric immersed in NaOH solution (pH = 14) are shown in Fig. 8b. Unlike the anti-acid test, a small part of the C-Fabric was wetted by the base solution for an immersion time of 1 hour. Three hours later, the whole C-Fabric sank to the bottom of the beaker. When water was placed onto the etched-sample, the water droplet quickly spread out, indicating that the treated-sample was superhydrophilic. From the SEM image of fabric@F-B(A)-S immersed in base solution (Fig. 8d), the nanostructure is observed to be seriously destroyed, with only a few SiO_2 particles remaining. Therefore, the fabric@F-B(A)-S coating has a low durability to alkali resistance. However, when the tested-sample was immersed in fluoroalkyl silane for 10 min and then cured at 135 °C for 30 min, the superhydrophobicity could be recovered.

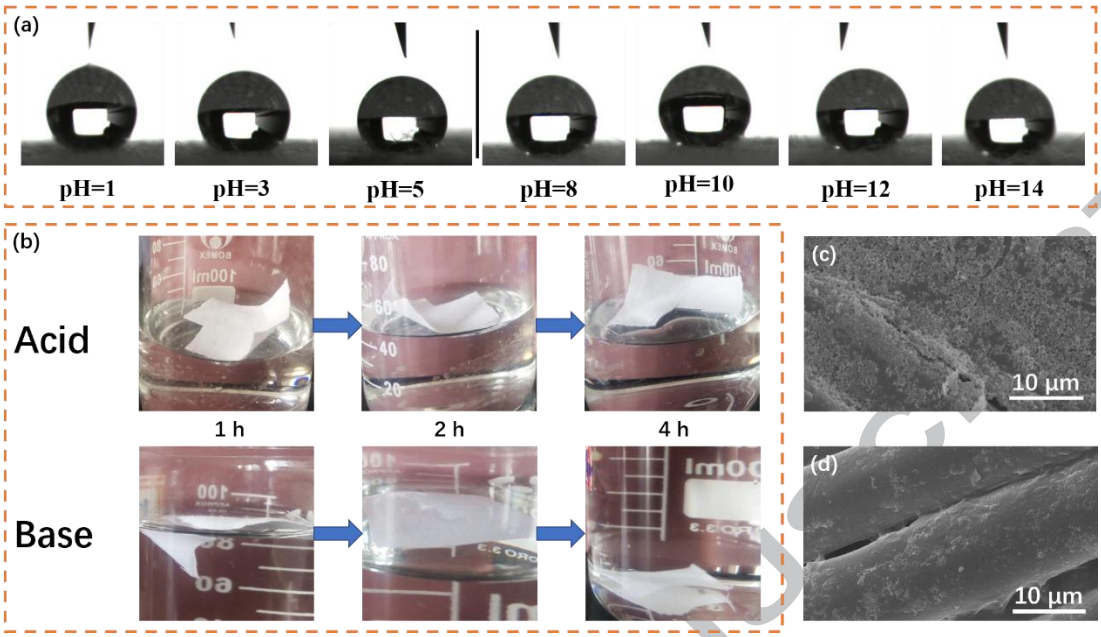

Fig. 8. (a) Shapes of different pH solution droplets on the superhydrophobic fabric@F-B(A)-S; (b) Photographs of the C-fabric immersed in H_2SO_4 (pH = 1) /NaOH (pH = 14) solution for 1, 2 and 4 hours; SEM image of the C-fabric after immersion in (c) H_2SO_4 solution and (d) NaOH solution for 4 hours

3.5 Thermal, UV and anti-smudge durability

In addition to the acid and base durability, it is very essential to explore durability to other damage such as thermal, UV and pollutant for evaluating the potential for extensive applications of this superhydrophobic coating. For thermal durability, the fabric@F-B(A)-S was treated in an air-circulating oven at 200 °C for 4 hours. After the heat treatment, as shown in Fig. 9a, the color of the C-Fibers deepened, with some light yellow spots appearing on the surface. However, when the blue water was placed onto the surface of the heat-treated C-Fabric, liquid balls formed, with the WCA maintained at 166°. Almost no difference exists between the fabric@F-B(A)-S before

and after treatment. The outstanding thermal stabilities of epoxy matrix and high crosslinking network ensure the excellent thermal durability of this superhydrophobic coating.

The coating was exposed to UV light at room temperature, with the wetting behavior of the fabric@F-B(A)-S recorded every hour. Fig. S11 shows the curves obtained for the CAs to water, ethylene glycol and oil for varying irradiation times. Almost no changes in the contact angles are found. After UV irradiating for 4 hours, the CA to water, glycol and oil was 163°, 146° and 143°, respectively, suggesting the superior anti-UV ability of fabric@F-B(A)-S (Movie S2), which results from the outstanding anti-UV performance of the C-F and Si-O bonds.

Common household liquids were also placed onto the surface of P-Fabric and C-Fabric, respectively. All of these liquids appeared as round-shaped balls on the C-Fibers but penetrated into the P-Fabric (Fig. 9b–c). This confirms that fabric@F-B(A)-S has outstanding antifouling abilities. Maxwell soluble coffee was utilized as pollutant to further evaluate the anti-smudge durability of fabric@F-B(A)-S. As shown in Fig. 9d, the state of the coating barely changes: no matter the immersion time, the fabric always floats on top of the coffee solution. The fluorinated chains of T-FAE prevent from the penetration of coffee droplets result in great anti-smudge durability.

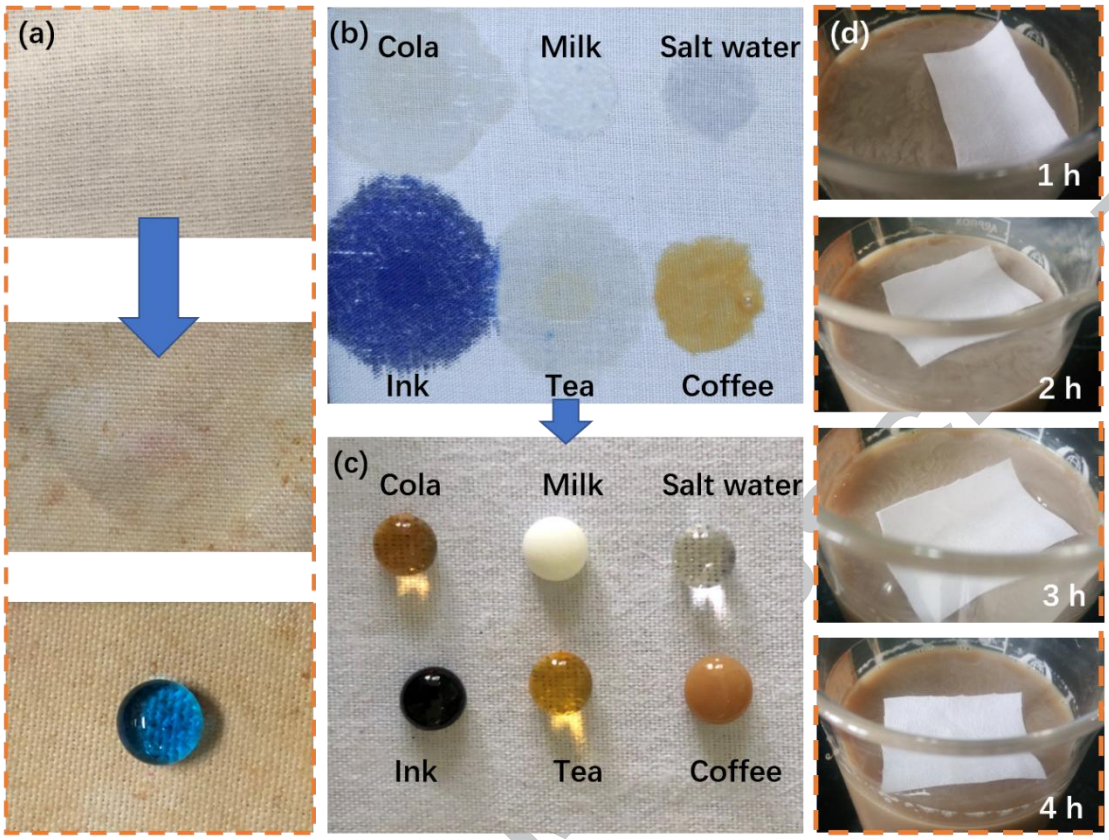

Fig. 9. (a) Photographs of the C-fabric taken before and after thermal treatment, with the blue water observed to remain on the surface of the treated C-fabric; photographs of common household solution droplets residing on the surface of (b) P-fabric (c) C-fabric; (d) Photographs of the C-fabric immersed in coffee solution for 1, 2, 3 and 4 hours

4. Conclusion

In summary, a novel branched epoxy named T-FAE, which contains an epoxy group and long fluoroalkyl chain in one molecule, was designed and synthesized. Based on this branched epoxy, robust superhydrophobic fabric coatings were successfully fabricated. For fabric@F-B(A)-S, the CA to water, glycol and colza oil was measured to be 165°, 147° and 144°, respectively, demonstrating superhydrophobicity. This coating can withstand at least 1000 abrasion cycles under

45 kPa. After the abrasion test, a WCA of 152° was maintained; the coating also showed a remarkable durability towards strong acid, UV light, thermal and smudge treatment without apparently losing its superhydrophobicity.

Acknowledgements

The Authors are grateful for financial support provided by the Science and Technology Project of ShenZhen (No. JCYJ20170306154725569), Science Foundation of Aeronautics of China (No. 2016ZF53059), and Key Project of Shanghai Space Foundation (No. SAST2016051)

Reference

[1] L. Feng, S. Li, Y. Li, H. Li, L. Zhang, J. Zhai, Y. Song, B. Liu, L. Jiang, D. Zhu, Super-hydrophobic surfaces: from natural to artificial, Adv. Mater. 14 (2002) 1857-1860.

[2] D.L. Hu, B. Chan, J.W. Bush, The hydrodynamics of water strider locomotion, Nature 424 (2003) 663-666.

[3] X. Gao, L. Jiang, Biophysics: water-repellent legs of water striders, Nature 432 (2004) 36-36.

[4] R. Blossey, Self-cleaning surfaces-virtual realities, Nat. Mater. 2 (2003) 301-306.

[5] H. Bellanger, T. Darmanin, E. T. de Givenchy, F. Guittard, Chemical and physical pathways for the preparation of superoleophobic surfaces and related wetting theories, Chem. Rev. 114 (2014) 2694-2716.

[6] S. Wang, K. Liu, X. Yao, L. Jiang, Bioinspired surfaces with superwettability: new

insight on theory, design, and applications, Chem. Rev. 115 (2015) 8230-8293.

[7] S. Wang, L. Jiang, Definition of superhydrophobic states, Adv. Mater. 19 (2007) 3423-3424.

[8] J. Li, L. Yan, Q. Ouyang, F. Zha, Z. Jing, X. Li, Z. Lei, Facile fabrication of translucent superamphiphobic coating on paper to prevent liquid pollution, Chem. Eng. J. 246 (2014) 238-243.

[9] T. Kamegawa, Y. Shimizu, H. Yamashita, Superhydrophobic Surfaces with Photocatalytic Self-Cleaning Properties by Nanocomposite Coating of TiO_2 and Polytetrafluoroethylene, Adv. Mater. 24 (2012) 3697-3700.

[10] C.H. Xue, Y.R. Li, P. Zhang, J.Z. Ma, S.T. Jia, Washable and wear-resistant superhydrophobic surfaces with self-cleaning property by chemical etching of fibers and hydrophobization, ACS Appl. Mater. Interf. 6 (2014) 10153-10161.

[11] C.R. Crick, J.C. Bear, A. Kafizas, I.P. Parkin, Superhydrophobic photocatalytic surfaces through direct incorporation of titania nanoparticles into a polymer matrix by aerosol assisted chemical vapor deposition, Adv. Mater. 24 (2012) 3505-3508.

[12] Y. Wang, J. Xue, Q. Wang, Q. Chen, J. Ding, Verification of icephobic/anti-icing properties of a superhydrophobic surface, ACS Appl. Mater. Interf. 5 (2013) 3370-3381.

[13] J. Lv, Y. Song, L. Jiang, J. Wang, Bio-inspired strategies for anti-icing, ACS nano 8 (2014) 3152-3169.

[14] L. Wang, Q. Gong, S. Zhan, L. Jiang, Y. Zheng, Robust Anti-Icing Performance of a Flexible Superhydrophobic Surface, Adv. Mater. 28 (2016) 7729-7735.

[15] A.C.C. de Leon, R.B. Pernites, R.C. Advincula, Superhydrophobic colloidally textured polythiophene film as superior anticorrosion coating, ACS Appl. Mater. Interf. 4 (2012) 3169-3176.

[16] F. Zhang, L. Zhao, H. Chen, S. Xu, D.G. Evans, X. Duan, Corrosion resistance of superhydrophobic layered double hydroxide films on aluminum, Angew. Chem. Int. Ed. 47 (2008) 2466-2469.

[17] K. Liu, L. Jiang, Metallic surfaces with special wettability, Nanoscale 3 (2011) 825-838.

[18] G.B. Hwang, A. Patir, K. Page, Y. Lu, E. Allan, I.P. Parkin, Buoyancy increase and drag-reduction through a simple superhydrophobic coating, Nanoscale (2017).

[19] M.N. Kavalenka, F. Vüllers, S. Lischker, C. Zeiger, A. Hopf, M. Röhrig, B.E. Rapp, M. Worgull, H. Hölscher, Bioinspired air-retaining nanofur for drag reduction, ACS Appl. Mater. Interf. 7 (2015) 10651-10655.

[20] Z. Xu, Y. Zhao, H. Wang, X. Wang, T. Lin, A Superamphiphobic Coating with an Ammonia-Triggered Transition to Superhydrophilic and Superoleophobic for Oil-Water Separation, Angew. Chem. 127 (2015) 4610-4613.

[21] L. Feng, Z. Zhang, Z. Mai, Y. Ma, B. Liu, L. Jiang, D. Zhu, A super-hydrophobic and super-oleophilic coating mesh film for the separation of oil and water, Angew. Chem. Int. Ed. 43 (2004) 2012-2014.

[22] D. Zang, F. Liu, M. Zhang, X. Niu, Z. Gao, C. Wang, Superhydrophobic coating on fiberglass cloth for selective removal of oil from water, Chem. Eng. J. 262 (2015) 210-216.

[23] U. Zulfiqar, S.Z. Hussain, M. Awais, M.M.J. Khan, I. Hussain, S.W. Husain, T. Subhani, In-situ synthesis of bi-modal hydrophobic silica nanoparticles for oil-water separation, Colloids Surf. A Physicochem. Eng. Asp. 508 (2016) 301-308.

[24] B. Bhushan, Y.C. Jung, K. Koch, Micro-, nano-and hierarchical structures for superhydrophobicity, self-cleaning and low adhesion, Philos. Trans. R. Soc. A 367 (2009) 1631-1672.

[25] H.Y. Erbil, A.L. Demirel, Y. Avcı, O. Mert, Transformation of a simple plastic into a superhydrophobic surface, Science 299 (2003) 1377-1380.

[26] L. Xu, D. Zhu, X. Lu, Q. Lu, Transparent, thermally and mechanically stable superhydrophobic coating prepared by an electrochemical template strategy, J. Mater. Chem. A 3 (2015) 3801-3807.

[27] L. Zhang, C.H. Xue, M. Cao, M.M. Zhang, M. Li, J.Z. Ma, Highly transparent fluorine-free superhydrophobic silica nanotube coatings, Chem. Eng. J. 320 (2017) 244-252.

[28] C.H. Wang, Y.Y. Song, J.W. Zhao, X.H. Xia, Semiconductor supported biomimetic superhydrophobic gold surfaces by the galvanic exchange reaction, Surf. Sci. 600 (2006) 38-42.

[29] X. Fan, X. Jia, H. Zhang, B. Zhang, C. Li, Q. Zhang, Synthesis of raspberry-like poly (styrene-glycidyl methacrylate) particles via a one-step soap-free emulsion polymerization process accompanied by phase separation, Langmuir 29 (2013) 11730-11741.

[30] Z. Liu, H. Wang, X. Zhang, C. Wang, C. Lv, Y. Zhu, Durable and self-healing

superhydrophobic surface with bistratal gas layers prepared by electrospinning and hydrothermal processes, Chem. Eng. J. 326 (2017) 578-586.

[31] Y. Qi, Z. Cui, B. Liang, R.S. Parnas, H. Lu, A fast method to fabricate superhydrophobic surfaces on zinc substrate with ion assisted chemical etching, Appl. Surf. Sci.305 (2014) 716-724.

[32] C.E. Hoyle, A.B. Lowe, C.N. Bowman, Thiol-click chemistry: a multifaceted toolbox for small molecule and polymer synthesis, Chem. Soc. Rev. 39 (2010) 1355-1387.

[33] S. Kostić, J.K. Berg, K. Casdorff, V. Merk, I. Burgert, E. Cabane, A straightforward thiol–ene click reaction to modify lignocellulosic scaffolds in water, Green Chem. 19 (2017) 4017-4022.

[34] J. Guo, W. Fang, A. Welle, W. Feng, I. Filpponen, O.J. Rojas, P.A. Levkin, Superhydrophobic and Slippery Lubricant-Infused Flexible Transparent Nanocellulose Films by Photoinduced Thiol–Ene Functionalization, ACS Appl. Mater. Interf. 8 (2016) 34115-34122.

[35] B.J. Sparks, E.F. Hoff, L. Xiong, J.T. Goetz, D.L. Patton, Superhydrophobic hybrid inorganic-organic thiol-ene surfaces fabricated via spray-deposition and photopolymerization, ACS Appl. Mater. Interf. 5 (2013) 1811-1817.

[36] T. Verho, C. Bower, P. Andrew, S. Franssila, O. Ikkala, R.H. Ras, Mechanically durable superhydrophobic surfaces, Adv. Mater. 23 (2011) 673-678.

[37] C.H. Xue, J.Z. Ma, Long-lived superhydrophobic surfaces, J. Mater. Chem. A 1 (2013) 4146-4161.

[38] D.S. Facio, M.J. Mosquera, Simple strategy for producing superhydrophobic nanocomposite coatings in situ on a building substrate, ACS Appl. Mater. Interf. 5 (2013) 7517-7526.

[39] C.W. Peng, K.C. Chang, C.J. Weng, M.C. Lai, C.H. Hsu, S.C. Hsu, S.Y. Li, Y. Wei, J.-M. Yeh, UV-curable nanocasting technique to prepare bio-mimetic super-hydrophobic non-fluorinated polymeric surfaces for advanced anticorrosive coatings, Polym. Chem. 4 (2013) 926-932.

[40] J. Wu, J. Li, Z. Wang, M. Yu, H. Jiang, L. Li, B. Zhang, Designing breathable superhydrophobic cotton fabrics, RSC Advances 5 (2015) 27752-27758.

[41] X. Zhang, Y. Si, J. Mo, Z. Guo, Robust micro-nanoscale flowerlike ZnO/epoxy resin superhydrophobic coating with rapid healing ability, Chem. Eng. J. 313 (2017) 1152-1159.

[42] F. Xue, D. Jia, Y. Li, X. Jing, Facile preparation of a mechanically robust superhydrophobic acrylic polyurethane coating, J. Mater. Chem. A 3 (2015) 13856-13863.

[43] B. Chen, J. Qiu, E. Sakai, N. Kanazawa, R. Liang, H. Feng, Robust and superhydrophobic surface modification by a “Paint+ Adhesive” method: applications in self-cleaning after oil contamination and oil–water separation, ACS Appl. Mater. Interf. 8 (2016) 17659-17667.

Highlight:

- A novel branched monomer called T-FAE was designed and synthesized.
- T-FAE contained epoxy group and long-fluorine in one molecule.
- The WCA of T-FAE coating is 165°.
- After the 1000 cycles abrasion test, its WCA could also maintain 152°.